

Next-to-leading order QCD corrections to the top quark associated with γ production via model-independent flavor-changing neutral-current couplings at hadron colliders

Yue Zhang, Bo Hua Li, Chong Sheng Li,^{*} Jun Gao, and Hua Xing Zhu

*Department of Physics and State Key Laboratory of Nuclear Physics and Technology,
Peking University, Beijing 100871, China*

(Dated: June 23, 2018)

Abstract

We present the complete next-to-leading order (NLO) QCD corrections to the top quark associated with γ production induced by model-independent $tq\gamma$ and tqg flavor-changing neutral-current (FCNC) couplings at hadron colliders, respectively. We also consider the mixing effects between the $tq\gamma$ and tqg FCNC couplings for this process. Our results show that, for the $tq\gamma$ couplings, the NLO QCD corrections can enhance the total cross sections by about 50% and 40% at the Tevatron and LHC, respectively. Including the contributions from the $tq\gamma$, tqg FCNC couplings and their mixing effects, the NLO QCD corrections can enhance the total cross sections by about 50% for the $tu\gamma$ and tug FCNC couplings, and by about the 80% for the $tc\gamma$ and tcg FCNC couplings at the LHC, respectively. Moreover, the NLO corrections reduce the dependence of the total cross section on the renormalization and factorization scale significantly. We also evaluate the NLO corrections for several important kinematic distributions.

PACS numbers: 14.65.Ha, 12.38.Bx, 12.60.Cn

^{*}Electronic address: csli@pku.edu.cn

I. INTRODUCTION

Top quark is an excellent probe for the new physics beyond the standard model (SM), since it is the heaviest particle discovered so far, with a mass close to the electroweak (EW) symmetry breaking scale. Direct evidence for new physics at TeV scale may be not easy to find, while indirect evidence, such as modification of SM predictions originated from new physics interaction, are important as well. A good consideration is to investigate single top quark production process via the anomalous flavor-changing neutral-current (FCNC) coupling. The FCNC couplings are absent at the tree level, and occur through loop diagrams within the SM, which are further suppressed by the Glashow-Iliopoulos-Maiani (GIM) mechanism [1]. Therefore, within the SM, single top quark FCNC production is expected to have tiny cross section, and is probably unmeasurable at the CERN Large Hadron Collider (LHC). However, the single top quark production induced by the FCNC coupling can be enhanced significantly in some new physics models [2–7]. Top quark will be copiously produced at the LHC (about 10^8 per year), even in the initial low luminosity run ($\sim 10 \text{ fb}^{-1}/\text{year}$) 8×10^6 top quark pairs and 3×10^6 single top quarks will be produced yearly. With such large samples, precise measurements of single top quark production will be available and provide a good opportunity to discover the first hint of new physics by observing the FCNC couplings in the top quark sector.

In this paper, we study the single top quark associated with γ production induced by FCNC couplings in a model-independent way by using the effective Lagrangian. The relevant effective lagrangian up to dimension 5 consists of the following operators [8]:

$$\begin{aligned} \mathcal{L}_{\text{eff}} = & -e \sum_{q=u,c} \frac{\kappa_{tq}^{\gamma}}{\Lambda} \bar{q} \sigma^{\mu\nu} (f_{tq}^{\gamma} + i h_{tq}^{\gamma} \gamma_5) t A_{\mu\nu} \\ & -g_s \sum_{q=u,c} \frac{\kappa_{tq}^g}{\Lambda} \bar{q} \sigma^{\mu\nu} T^a (f_{tq}^g + i h_{tq}^g \gamma_5) t G_{\mu\nu}^a + \text{H.c.} \end{aligned} \quad (1)$$

where Λ is the new physics scale, $A_{\mu\nu}$ and $G_{\mu\nu}^a$ are the field strength tensors of photon and gluon respectively, and T^a are the conventional Gell-Mann matrices. κ_{tq}^V are real and positive, while f_{tq}^V and h_{tq}^V are complex numbers satisfying $|f_{tq}^V|^2 + |h_{tq}^V|^2 = 1$ with $V = \gamma, g$ and $q = u, c$.

Present experimental constraints for the $tq\gamma$ FCNC couplings come from the non-observation of the decays $t \rightarrow q\gamma$ at Tevatron and the absence of the single top production

$eu \rightarrow et$ at HERA. The CDF collaboration has set 95% confidence level (CL) limits on the branching fractions $\text{Br}(t \rightarrow q\gamma) \leq 0.032$ [9], which corresponds to $\kappa_{tq}^\gamma/\Lambda \leq 0.77\text{TeV}^{-1}$ based on the theoretical predictions of $t \rightarrow q + \gamma$ at the Next-to-leading order(NLO) level in QCD [10, 11]. The ZEUS collaboration also provides a more stringent constraints, $\kappa_{tu}^\gamma < 0.174$ at a 95% CL, through the measurements of $ep \rightarrow etX$ [12] using the NLO predictions [13], which can be transferred to $\kappa_{tu}^\gamma/\Lambda < 0.33\text{TeV}^{-1}$. Recently, the most stringent experimental constraints for the tqg FCNC couplings are $\kappa_{tu}^g/\Lambda \leq 0.013 \text{ TeV}^{-1}$ and $\kappa_{tc}^g/\Lambda \leq 0.057 \text{ TeV}^{-1}$ given by the D0 Collaboration [14], and $\kappa_{tu}^g/\Lambda \leq 0.018 \text{ TeV}^{-1}$ and $\kappa_{tc}^g/\Lambda \leq 0.069 \text{ TeV}^{-1}$ given by the CDF Collaboration [15], based on the measurements of the FCNC single top production using the theoretical predictions, including the NLO QCD corrections [16, 17] and resummation effects [18], respectively.

The observation of $qg \rightarrow \gamma t$ process is a clear signal of top quark FCNC interactions, which can be induced by $tq\gamma$ and tqg couplings, since there is no irreducible backgrounds of this process in the SM. There are already several literatures [19] discussing this process using effective Lagrangian Eq. (1). However they were either based on the LO calculations, or the NLO QCD effects are not completely calculated. So it is necessary to present a complete NLO corrections to the above process, which is not only mandatory for matching the expected experimental accuracy at hadron colliders, but is also important for a consistent treatment of both the top quark production and decay via the FCNC couplings by experiments.

In this paper, we present the complete NLO QCD corrections to the top quark associated with γ production via $tq\gamma$ and tqg FCNC couplings with their mixing effects at hadron colliders.

The arrangement of this paper is as follows. In Sec. II, we present the LO results for the top quark associated with γ production induced by the $tq\gamma$ FCNC couplings. In Sec. III, we show the details of the corresponding NLO calculations. Sec. IV contains the analysis of $qg \rightarrow \gamma t$ process induced by the the $tq\gamma$, tqg FCNC couplings and the mixing effects. We present the numerical results in Sec. V. Finally, we give our conclusion in Sec. VI.

II. LEADING ORDER RESULTS

At hadron colliders, there is only one process $qg \rightarrow \gamma t$ with $q = c, u$ that contributes to the $t\gamma$ associated production at the LO via the electroweak FCNC couplings, κ_{tq}^γ . The corresponding Feynman diagrams are shown in Fig. 1.

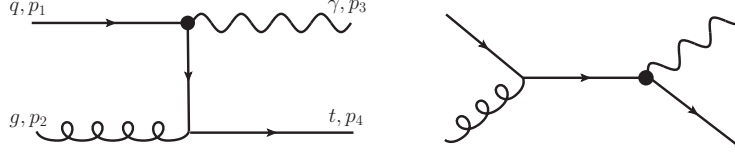


FIG. 1: The LO Feynman diagrams for top quark associated with γ production via the $tq\gamma$ FCNC couplings.

From the effective operator in Eq. (1), we obtain the following LO squared amplitudes for above process in four dimensions,

$$\begin{aligned} \overline{|M^B|^2}(s, t, u) = & \frac{64\pi^2\alpha_s\alpha}{3s(m^2 - t)^2} \left(\frac{\kappa_{tq}^\gamma}{\Lambda} \right)^2 \left[m^8 - (2s + t)m^6 + (s^2 + 4st + t^2)m^4 \right. \\ & \left. - (3s^2 + 6st + t^2)tm^2 + 2st^2(s + t) \right], \end{aligned} \quad (2)$$

where m is the top quark mass, the colors and spins of the outgoing particles have been summed over, and the colors and spins of the incoming ones have been averaged over, s , t , and u are Mandelstam variables, which are defined as

$$s = (p_1 + p_2)^2, \quad t = (p_1 - p_3)^2, \quad u = (p_1 - p_4)^2. \quad (3)$$

After the phase space integration, the LO partonic cross sections are given by

$$\hat{\sigma}_{ab}^B = \frac{1}{2\hat{s}} \int d\Gamma \overline{|M^B|^2}_{ab}. \quad (4)$$

The LO total cross section at hadron colliders is obtained by convoluting the partonic cross section with the parton distribution functions (PDFs) $G_{i/P}$ for the proton (antiproton):

$$\sigma^B = \sum_{ab} \int dx_1 dx_2 [G_{a/P_1}(x_1, \mu_f) G_{b/P_2}(x_2, \mu_f) \hat{\sigma}_{ab}^B], \quad (5)$$

where μ_f is the factorization scale.

III. NEXT-TO-LEADING ORDER QCD CORRECTIONS

In this section, we present our calculations for the NLO QCD corrections to the top quark associated with γ production via the electroweak FCNC couplings. At the NLO, we need to include contributions from both the virtual corrections (Fig. 2) and the real corrections (Fig. 3). We use the dimensional regularization scheme (with naive γ_5) in $n = 4 - 2\epsilon$ dimensions to regularize both ultraviolet (UV) and infrared (IR) divergence. Moreover, for the real corrections, we used the dipole subtraction method with massive partons [20, 21] to separate the IR divergence.

All the UV divergence appearing in the loop diagrams are canceled by introducing counterterms for the wave functions and mass of the external fields ($\delta Z_2^{(g)}, \delta Z_2^{(q)}, \delta Z_2^{(t)}, \delta m$), and the coupling constants ($\delta Z_{gs}, \delta Z_{\kappa_{tq}^\gamma/\Lambda}$). We define these counterterms according to the same procedures adopted in Ref.[16]:

$$\begin{aligned}\delta Z_2^{(g)} &= -\frac{\alpha_s}{2\pi} C_\epsilon \left(\frac{N_f}{3} - \frac{5}{2} \right) \left(\frac{1}{\epsilon_{UV}} - \frac{1}{\epsilon_{IR}} \right) - \frac{\alpha_s}{6\pi} C_\epsilon \frac{1}{\epsilon_{UV}}, \\ \delta Z_2^{(q)} &= -\frac{\alpha_s}{3\pi} C_\epsilon \left(\frac{1}{\epsilon_{UV}} - \frac{1}{\epsilon_{IR}} \right), \\ \delta Z_2^{(t)} &= -\frac{\alpha_s}{3\pi} C_\epsilon \left(\frac{1}{\epsilon_{UV}} + \frac{2}{\epsilon_{IR}} + 4 \right), \\ \delta Z_{gs} &= \frac{\alpha_s}{4\pi} \Gamma(1+\epsilon) (4\pi)^\epsilon \left(\frac{N_f}{3} - \frac{11}{2} \right) \frac{1}{\epsilon_{UV}} + \frac{\alpha_s}{12\pi} C_\epsilon \frac{1}{\epsilon_{UV}},\end{aligned}\tag{6}$$

where $C_\epsilon = \Gamma(1+\epsilon)[(4\pi\mu_r^2)/m^2]^\epsilon$ and $n_f = 5$. For δm , we use the on-shell subtraction:

$$\frac{\delta m}{m} = -\frac{\alpha_s}{3\pi} C_\epsilon \left(\frac{3}{\epsilon_{UV}} + 4 \right),\tag{7}$$

And, we adopt the $\overline{\text{MS}}$ scheme for the renormalization constants of the electroweak FCNC couplings $\delta Z_{\kappa_{tq}^\gamma/\Lambda}$, and adjust it to cancel the remaining UV divergence exactly:

$$\delta Z_{\kappa_{tq}^\gamma/\Lambda} = \frac{\alpha_s}{3\pi} \Gamma(1+\epsilon) (4\pi)^\epsilon \frac{1}{\epsilon_{UV}},\tag{8}$$

Here we first consider the electroweak FCNC couplings, the running of the couplings are given by [11]

$$\kappa^\gamma(\mu) = \kappa^\gamma(\mu') \eta^{\frac{4}{3\beta_0}},\tag{9}$$

where $\eta = \alpha_s(\mu')/\alpha_s(\mu)$ and β_0 is the 1-loop QCD β -function given by $11 - \frac{2}{3}n_f$ with n_f active flavors between the two scales μ and μ' .

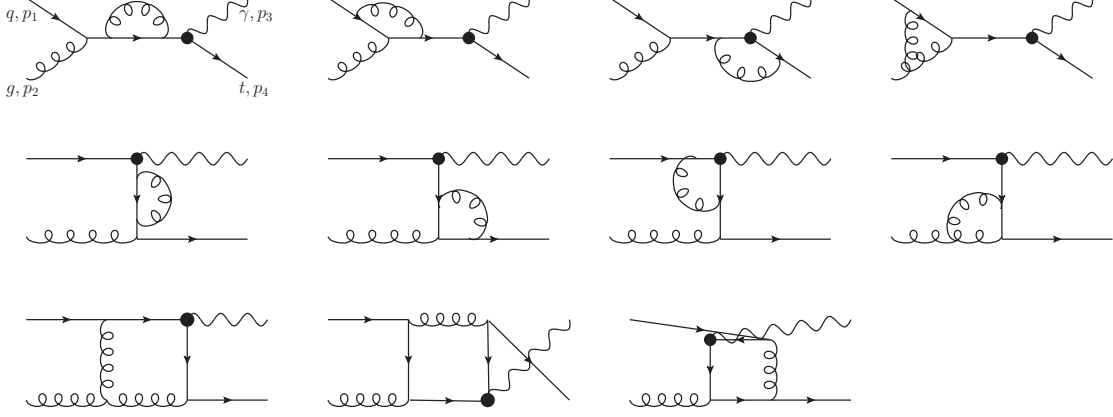


FIG. 2: One-loop Feynman diagrams for the process $qg \rightarrow \gamma t$ induced by the $tq\gamma$ FCNC couplings.

The squared amplitudes of the virtual corrections are

$$\overline{|M|^2}_{1-loop} = \sum_i 2Re(\overline{M^{loop,i} M^{B*}}) + 2Re(\overline{M^{con} M^{B*}}), \quad (10)$$

where $M^{loop,i}$ denote the amplitudes for the i -th loop diagram in Fig. 2, and M^{con} are the corresponding counterterms. All the UV divergence in Eq. (10) have been cancelled as they must, but the IR divergent pieces are still present. Because of the limited space, we do not show the lengthy explicit expressions of the virtual corrections here. The IR divergence of the virtual corrections can be factorized as

$$\overline{|M|^2}_{one-loop,IR} = -\frac{\alpha_s}{12\pi} D_\epsilon \left\{ \frac{13}{\epsilon_{IR}^2} + \left[9 \ln\left(\frac{s}{m^2}\right) + 9 \ln\left(\frac{m^2-t}{m^2}\right) - \ln\left(\frac{s+t}{m^2}\right) + \frac{43}{2} \right] \frac{1}{\epsilon_{IR}} \right\} \times \overline{|M^B|^2}, \quad (11)$$

where $D_\epsilon = [(4\pi\mu_r^2)/m^2]^\epsilon/\Gamma(1-\epsilon)$, and $\overline{|M^B|^2}$ are the squared Born amplitudes given in Eq. (2).

At the NLO the real corrections consist of the radiations of an additional gluon or massless (anti)quark in the final states, including the subprocesses

$$\begin{aligned} q g &\rightarrow \gamma t g, \quad g g \rightarrow \gamma t \bar{q}, \quad q \bar{q} \rightarrow \gamma t \bar{q}, \\ q q &\rightarrow \gamma t q, \quad q q' \rightarrow \gamma t q', \quad q' \bar{q}' \rightarrow \gamma t \bar{q}, \end{aligned} \quad (12)$$

here q denotes u quark for the κ_{tu}^γ coupling and c quark for the κ_{tc}^γ coupling, while q' denotes massless (anti)quark other than q . It should be noted that in our NLO calculations we do not include the contributions from the SM on-shell production of the top pair with subsequent

rare decay of one top quark, $pp(\bar{p}) \rightarrow t\bar{t} \rightarrow \gamma + t + \bar{q}$, which provide the same signature as the top quark associated with γ production via the FCNC couplings and can be calculated separately.

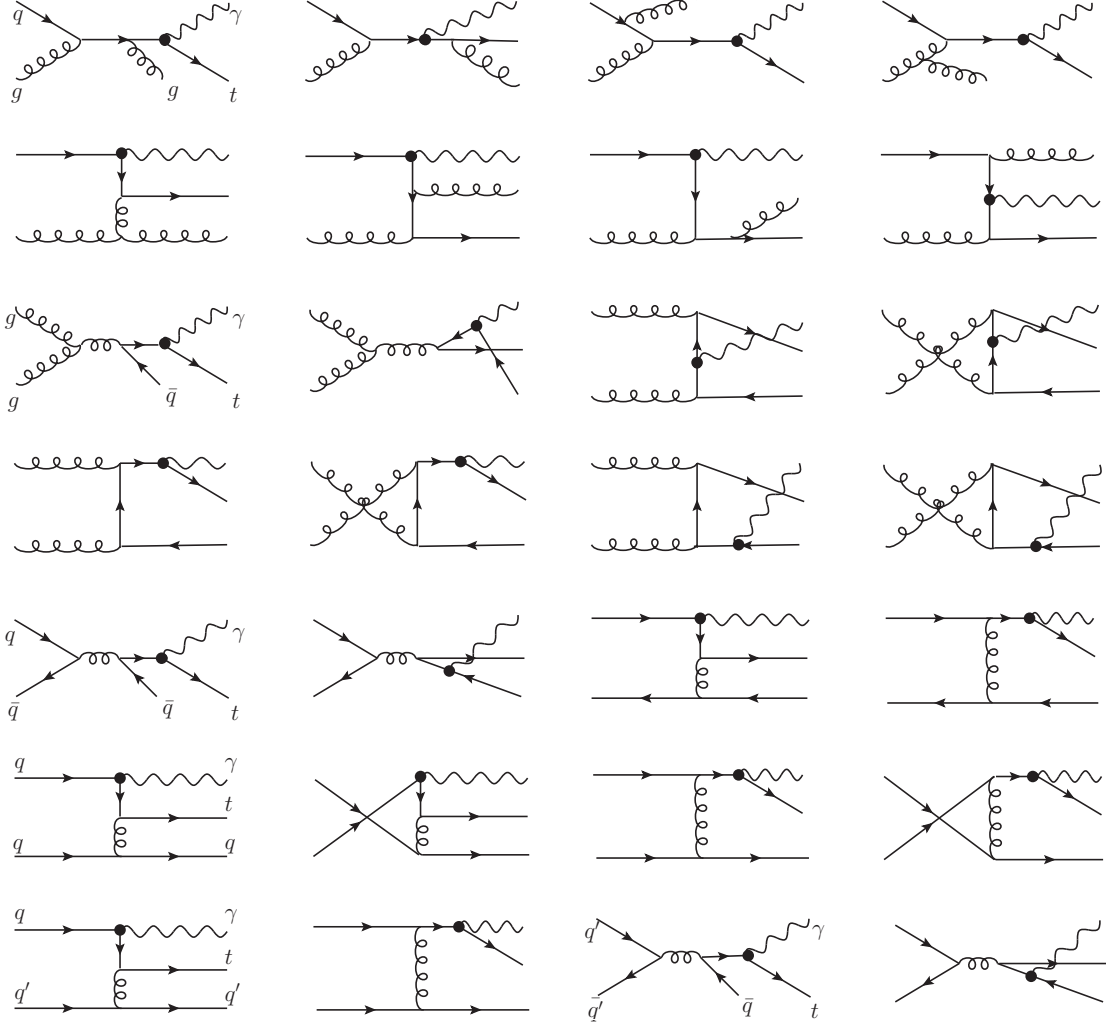


FIG. 3: Feynman diagrams of the real corrections induced by the $tq\gamma$ FCNC couplings.

Before performing the numerical calculations, we need to extract the IR divergences in the real corrections. In the dipole formalism this is done by subtracting some dipole terms from the real corrections to cancel the singularities exactly, such that the real corrections become integrable in four dimensions. These dipole subtraction terms are analytically integrable in n dimensions over one-parton subspaces, which give ϵ poles that represent the soft and collinear divergences. Then we can add them to the virtual corrections to cancel the ϵ poles, and ensure the virtual corrections are also integrable in four dimensions. This whole

procedure can be illustrated by the formula [21]:

$$\hat{\sigma}^{NLO} = \int_{m+1} [(d\hat{\sigma}^R)_{\epsilon=0} - (d\hat{\sigma}^A)_{\epsilon=0}] + \int_m \left[d\hat{\sigma}^V + \int_1 d\hat{\sigma}^A \right]_{\epsilon=0}, \quad (13)$$

where m is the number of final state particles at the LO, and $d\hat{\sigma}^A$ is a sum of the dipole terms. Besides, at hadron colliders, we have to include the well-known collinear subtraction counterterms in order to cancel the collinear divergences arising from the splitting processes of the initial state massless partons. Here we use the $\overline{\text{MS}}$ scheme and the corresponding NLO PDFs.

For the process with two initial state hadrons, the dipole terms can be classified into four groups, the final-state emitter and final-state spectator type,

$$\begin{aligned} \mathcal{D}_{ij,k}(p_1, \dots, p_{m+1}) = \\ - \frac{1}{(p_i + p_j)^2 - m_{ij}^2} {}_m \langle \dots, \tilde{i}j, \dots, \tilde{k}, \dots | \frac{\mathbf{T}_k \cdot \mathbf{T}_{ij}}{\mathbf{T}_{ij}^2} \mathbf{V}_{ij,k} | \dots, \tilde{i}j, \dots, \tilde{k}, \dots \rangle_m, \end{aligned} \quad (14)$$

the final-state emitter and initial-state spectator type,

$$\begin{aligned} \mathcal{D}_{ij}^a(p_1, \dots, p_{m+1}; p_a, \dots) = \\ - \frac{1}{(p_i + p_j)^2 - m_{ij}^2} \frac{1}{x_{ij,a}} {}_{m,a} \langle \dots, \tilde{i}j, \dots, \tilde{a}, \dots | \frac{\mathbf{T}_a \cdot \mathbf{T}_{ij}}{\mathbf{T}_{ij}^2} \mathbf{V}_{ij}^a | \dots, \tilde{i}j, \dots, \tilde{a}, \dots \rangle_{m,a}, \end{aligned} \quad (15)$$

the initial-state emitter and final-state spectator type,

$$\begin{aligned} \mathcal{D}_j^{ai}(p_1, \dots, p_{m+1}; p_a, \dots) = \\ - \frac{1}{2p_a p_i} \frac{1}{x_{ij,a}} {}_{m,\tilde{a}i} \langle \dots, \tilde{j}, \dots, \tilde{a}i, \dots | \frac{\mathbf{T}_j \cdot \mathbf{T}_{ai}}{\mathbf{T}_{ai}^2} \mathbf{V}_j^{ai} | \dots, \tilde{j}, \dots, \tilde{a}i, \dots \rangle_{m,\tilde{a}i}, \end{aligned} \quad (16)$$

and the initial-state emitter and initial-state spectator type,

$$\begin{aligned} \mathcal{D}^{ai,b}(p_1, \dots, p_{m+1}; p_a, p_b) = \\ - \frac{1}{2p_a p_i} \frac{1}{x_{i,ab}} {}_{m,\tilde{a}i} \langle \dots, \tilde{a}i, b | \frac{\mathbf{T}_b \cdot \mathbf{T}_{ai}}{\mathbf{T}_{ai}^2} \mathbf{V}^{ai,b} | \dots, \tilde{a}i, b \rangle_{m,\tilde{a}i}, \end{aligned} \quad (17)$$

where a, b and i, j, \dots are the initial and final state partons, and \mathbf{T} and \mathbf{V} are the color charge operators and dipole functions acting on the LO amplitudes, respectively. The explicit expressions for $x_{i,ab}$, $x_{ij,a}$ and \mathbf{V} can be found in Ref. [21]. The integrated dipole functions together with the collinear counterterms can be written in the following factorized form

$$\begin{aligned} \sim & \int d\Phi^{(m)}(p_a, p_b) {}_{m,ab} \langle \dots; p_a, p_b | \mathbf{I}_{m+a+b}(\epsilon) | \dots; p_a, p_b \rangle_{m,ab} \\ & + \sum_{a'} \int_0^1 dx \int d\Phi^{(m)}(xp_a, p_b) {}_{m,a'b} \langle \dots; xp_a, p_b | \mathbf{P}_{m+b}^{a,a'}(x) + \mathbf{K}_{m+b}^{a,a'}(x) | \dots; xp_a, p_b \rangle_{m,a'b} \\ & + (a \leftrightarrow b), \end{aligned} \quad (18)$$

where x is the momentum fraction of the splitting parton, $d\Phi^{(m)}$ contains all the factors apart from the squared amplitudes, \mathbf{I} , \mathbf{P} , and \mathbf{K} are insertion operators defined in [21].

The operators \mathbf{P} and \mathbf{K} provide finite contributions to the NLO corrections, and only the operator \mathbf{I} contains the IR divergences

$$\begin{aligned} \mathbf{I}|_{IR} = & -\frac{\alpha_s}{2\pi} \frac{(4\pi)^\epsilon}{\Gamma(1-\epsilon)} \left\{ \sum_j \sum_{k \neq j} \mathbf{T}_j \cdot \mathbf{T}_k \left[\left(\frac{\mu_r^2}{s_{jk}} \right)^\epsilon \mathcal{V}(s_{jk}, m_j, m_k; \epsilon_{IR}) + \frac{1}{\mathbf{T}_j^2} \Gamma_j(m_j, \epsilon_{IR}) \right] \right. \\ & + \sum_j \mathbf{T}_j \cdot \mathbf{T}_a \left[2 \left(\frac{\mu_r^2}{s_{ja}} \right)^\epsilon \mathcal{V}(s_{ja}, m_j, 0; \epsilon_{IR}) + \frac{1}{\mathbf{T}_j^2} \Gamma_j(m_j, \epsilon_{IR}) + \frac{1}{\mathbf{T}_a^2} \frac{\gamma_a}{\epsilon_{IR}} \right] \\ & \left. + \mathbf{T}_a \cdot \mathbf{T}_b \left[\left(\frac{\mu_r^2}{s_{ab}} \right)^\epsilon \left(\frac{1}{\epsilon_{IR}^2} + \frac{1}{\mathbf{T}_a^2} \frac{\gamma_a}{\epsilon_{IR}} \right) \right] + (a \leftrightarrow b) \right\}, \end{aligned} \quad (19)$$

with

$$\begin{aligned} \mathcal{V}(s_{jk}, m_j, m_k; \epsilon_{IR}) &= \frac{1}{v_{jk}} \left(\frac{Q_{jk}^2}{s_{jk}} \right)^\epsilon \times \left(1 - \frac{1}{2} \rho_j^{-2\epsilon} - \frac{1}{2} \rho_k^{-2\epsilon} \right) \frac{1}{\epsilon_{IR}^2}, \\ \Gamma_j(0, \epsilon_{IR}) &= \frac{\gamma_j}{\epsilon_{IR}}, \quad \Gamma_j(m_j \neq 0, \epsilon_{IR}) = \frac{C_F}{\epsilon_{IR}}, \end{aligned} \quad (20)$$

where $C_F = 4/3$, $\gamma_q = 2$, and $\gamma_g = 11/2 - n_f/3$. And s_{jk} , Q_{jk}^2 , v_{jk} , and ρ_n are kinematic variables defined as follows

$$\begin{aligned} s_{jk} &= 2p_j p_k, \quad Q_{jk}^2 = s_{jk} + m_j^2 + m_k^2, \quad v_{jk} = \sqrt{1 - \frac{m_j^2 m_k^2}{(p_j p_k)^2}}, \\ \rho_n &= \sqrt{\frac{1 - v_{jk} + 2m_n^2/(Q_{jk}^2 - m_j^2 - m_k^2)}{1 + v_{jk} + 2m_n^2/(Q_{jk}^2 - m_j^2 - m_k^2)}} \quad (n = j, k). \end{aligned} \quad (21)$$

When inserting Eq. (19) into the LO amplitudes as shown in Eq. (18), we can see that the IR divergences can be written as combinations of the LO color correlated squared amplitudes and all the IR divergences from the virtual corrections in Eq. (11) are canceled exactly, as we expected.

In order to check our result, we have also performed the calculation with the two-cutoff method [22]. We find that the numerical results are in good agreement.

IV. CONTRIBUTIONS FROM THE ELECTROWEAK AND STRONG FCNC COUPLINGS WITH MIXING EFFECTS

In previous sections, we only consider the contributions from the electroweak FCNC couplings, κ_{tq}^γ . However, for the top quark associated γ production process, $qg \rightarrow \gamma t$,

there are additional contributions from the strong FCNC couplings, κ_{tq}^g , and the mixing effects between these two operators. Because the magnitudes of the coefficients κ_{tq}^V ($V = \gamma, g$) depend on the underlying new physics, these operator mixing contributions may be significant in certain models. Since the $\mathcal{O}(\alpha_s)$ corrections to the process $qg \rightarrow \gamma t$ induced by κ_{tq}^g are similar to the ones induced by κ_{tq}^γ , we don't show its analytical results, and only present the combination of the contributions from the $tq\gamma$, tqg and their mixing effects in this section.

In case that both of the κ_{tq}^g and κ_{tq}^γ are at the same order, the terms proportional to $(\kappa_{tq}^g)^2$, $\kappa^g \kappa^\gamma$ and $(\kappa_{tq}^\gamma)^2$ can contribute to $qg \rightarrow \gamma t$ with the same significance. The mixing terms, which are proportional to $\kappa^g \kappa^\gamma$, could appear in both the LO and NLO.

At the LO, there are four Feynman diagrams for this process, as shown in Fig. 4. Two of them are the same as Fig. 1, while the others are induced by κ_{qt}^g .

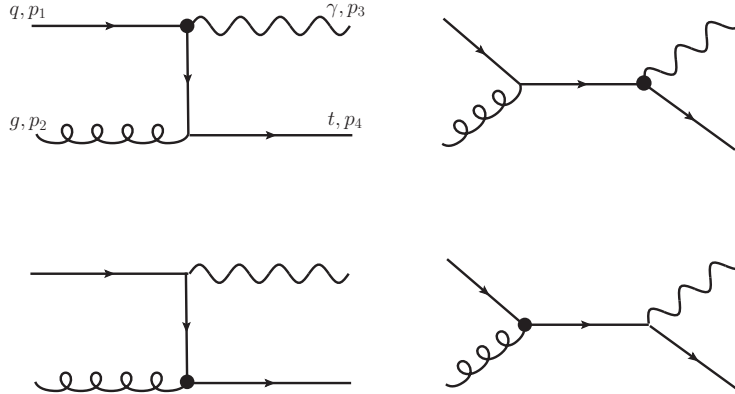


FIG. 4: The LO Feynman diagrams for top quark production associated with γ via the $tq\gamma$ and tqg FCNC couplings.

The complete LO squared amplitudes for this process in four dimensions are

$$\begin{aligned}
\overline{|M^B|_{tot}^2}(s, t, u) = & \frac{16\pi^2\alpha_s\alpha}{3} \left\{ \frac{4}{s(m^2-t)^2} \left(\frac{\kappa_{tq}^\gamma}{\Lambda} \right)^2 \left[m^8 - (2s+t)m^6 + (s^2+4st+t^2)m^4 \right. \right. \\
& - (3s^2+6st+t^2)tm^2 + 2st^2(s+t) \Big] \\
& + \frac{16}{9(m^2-s)^2t} \left(\frac{\kappa_{tq}^g}{\Lambda} \right)^2 \left[m^8 - (s+2t)m^6 + (s^2+4st+t^2)m^4 \right. \\
& - (s^2+6st+3t^2)sm^2 + 2s^2t(s+t) \Big] \\
& - \frac{16}{3(m^2-s)(m^2-t)} \left(\frac{\kappa_{tq}^g\kappa_{tq}^\gamma}{\Lambda^2} \right) \text{Re}(f_{tq}^{\gamma*}f_{tq}^g + h_{tq}^{\gamma*}h_{tq}^g) \left[3m^6 - 4(s+t)m^4 \right. \\
& \left. \left. + (s^2+3st+t^2)m^2 - st(s+t) \right] \right\}, \tag{22}
\end{aligned}$$

At the NLO, we need to include both the virtual corrections (Fig. 2, 13 and 14) and the real corrections (Fig. 3, 15 and 16). The relevant renormalization constants are the same as ones in Eqs. (6), (7) and (8), except that we introduce additional renormalization constants. We adopt the definition in Ref. [11]

$$\mathcal{L}_{\text{eff}} + \delta\mathcal{L}_{\text{eff}} = -(\kappa^g, \kappa^\gamma) \begin{pmatrix} 1 + \delta Z_{gg} & \delta Z_{g\gamma} \\ \delta Z_{\gamma g} & 1 + \delta Z_{\gamma\gamma} \end{pmatrix} \begin{pmatrix} O_g \\ O_\gamma \end{pmatrix}, \tag{23}$$

where the operators O_i ($i = g, \gamma$) are defined as $O_g = g_s \bar{q} \sigma^{\mu\nu} T^a (f_{tq}^g + i h_{tq}^g \gamma_5) t G_{\mu\nu}^a$, $O_\gamma = e \bar{q} \sigma^{\mu\nu} (f_{tq}^\gamma + i h_{tq}^\gamma \gamma_5) t A_{\mu\nu}$, and $\delta Z_{gg} = \delta Z_{\kappa_{tq}^g/\Lambda}$, $\delta Z_{\gamma\gamma} = \delta Z_{\kappa_{tq}^\gamma/\Lambda}$. At the $\mathcal{O}(\alpha_s)$ level, $\delta Z_{\kappa_{tq}^g/\Lambda}$ is presented in Eq. (8), and other renormalization constants are given by

$$\delta Z_{\kappa_{tq}^g/\Lambda} = \frac{\alpha_s}{6\pi} \Gamma(1+\epsilon) (4\pi)^\epsilon \frac{1}{\epsilon_{UV}}, \tag{24}$$

$$\delta Z_{g\gamma} = \frac{8\alpha_s}{9\pi} \Gamma(1+\epsilon) (4\pi)^\epsilon \frac{1}{\epsilon_{UV}}, \tag{25}$$

$$\delta Z_{\gamma g} = 0. \tag{26}$$

All the UV divergence are canceled exactly after the renormalization. The remaining IR divergence of the virtual corrections is the same as Eq. (11), except using the LO amplitude including the contributions from both the electroweak and the strong FCNC couplings instead of M^B .

For the real corrections, we still use the dipole subtraction method as in above section. We don't repeat the detailed description here. All the IR divergence from the virtual corrections are canceled exactly. A criterion for isolated photon has been suggested in Ref. [23], which

defines an IR-safe cross section decoupled with hadronic fragmentation and at the same time allows for complete cancelation of soft gluon divergence. For the case of only one final-state massless parton, such criterion is equivalent to the kinematic cut

$$p_T^j < \frac{1 - \cos \Delta R_{j\gamma}}{1 - \cos \Delta R_0} p_T^\gamma, \quad \text{for } \Delta R_{j\gamma} < \Delta R_0, \quad (27)$$

where j stands for either the final-state (anti-)quark or the final-state gluon. $\Delta R_{j\gamma}$ is the distance between the parton and the photon in the rapidity-azimuthal angle plane. We choose the cone-size parameters $\Delta R_0 = 0.7$ throughout our calculation.

When we consider the mixing effects, the running of κ^γ is different from the one without mixing effects. The running of κ^γ and κ^g are given by [11]:

$$\kappa^g(\mu) = \kappa^g(\mu') \eta^{\frac{2}{3\beta_0}}, \quad (28)$$

$$\kappa^\gamma(\mu) = \kappa^\gamma(\mu') \eta^{\frac{4}{3\beta_0}} + \frac{16}{3} \kappa^g(\mu') \left(\eta^{\frac{4}{3\beta_0}} - \eta^{\frac{2}{3\beta_0}} \right), \quad (29)$$

where $\eta = \alpha_s(\mu')/\alpha_s(\mu)$ and $\beta_0 = 11 - \frac{2}{3}n_f$ with $n_f = 5$.

V. NUMERICAL RESULTS

A. Process via the $tq\gamma$ FCNC couplings without mixing effects

Here we first consider the top associated with γ production via the $tq\gamma$ FCNC couplings, including the NLO QCD effects on the total cross sections, the scale dependence, and several important distributions at both the Tevatron and LHC. For the numerical calculations of this process, we take the SM parameters as follow [24]:

$$m_t = 172.0\text{GeV}, \quad \alpha_s(M_Z) = 0.118, \quad \alpha = 1/128.921. \quad (30)$$

And we set the electroweak FCNC couplings as:

$$\kappa_{tu}^\gamma/\Lambda = \kappa_{tc}^\gamma/\Lambda = 0.3\text{TeV}^{-1}. \quad (31)$$

The running QCD coupling constant is evaluated at the three-loop order [24] and the CTEQ6M PDF set [25] is used throughout the calculations of the NLO (LO) cross sections. Unless specified, both the renormalization and factorization scales are fixed to be the top quark mass. Besides, we impose the photon transverse momentum cut $p_T > 40\text{GeV}$

and pseudo-rapidity cut $|\eta| < 2.5$. We have performed two independent calculations for the virtual corrections and the integrated dipole terms, and used the modified MadDipole [26] package to generate the Fortran code for the real corrections. The numerical results of the two groups are in good agreement within the expected accuracy of our numerical program.

FCNC coupling	$tu\gamma$ (LO)	$tu\gamma$ (NLO)	$tc\gamma$ (LO)	$tc\gamma$ (NLO)
LHC $(\frac{\kappa/\Lambda}{0.3\text{TeV}^{-1}})^2$ pb	3.78	5.16	0.386	0.537
Tevatron $(\frac{\kappa/\Lambda}{0.3\text{TeV}^{-1}})^2$ fb	22.2	33.4	0.740	1.09

TABLE I: The LO and NLO total cross sections for the single top quark associated with γ production via the $tq\gamma$ FCNC couplings at both the LHC and Tevatron.

In Table I, we list some typical numerical results of the LO and NLO total cross sections for the top quark associated with γ production via the electroweak FCNC couplings.

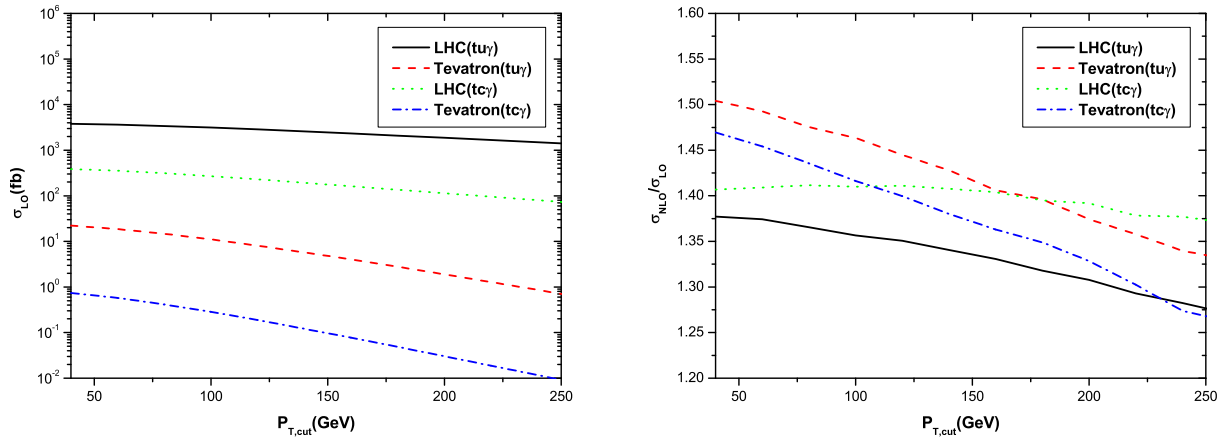


FIG. 5: The LO total cross sections and NLO K factors as functions of the photon transverse momentum cut.

In Fig. 5, we show the LO total cross sections and the K factors σ_{NLO}/σ_{LO} as functions of the photon transverse momentum cut, respectively. It can be seen that, for the $tc\gamma$ coupling the NLO corrections can enhance the total cross sections by about 50% and 40%, and for the $tu\gamma$ coupling by about 50% and 40% at the Tevatron and LHC, respectively. And the K factors decrease with the increasing transverse momentum cut.

In Fig. 6 and 7 we present the scale dependence of the LO and NLO total cross section for three cases: (1) the renormalization scale dependence $\mu_r = \mu$, $\mu_f = m_t$, (2) the factorization scale dependence $\mu_r = m_t$, $\mu_f = \mu$, and (3) total scale dependence $\mu_r = \mu_f = \mu$. It can be seen that the NLO corrections reduce the scale dependence significantly for all three cases, which make the theoretical predictions more reliable. For example, at the LHC for the $tu\gamma$ coupling, when the scale μ varies from $0.5m_t$ to $2m_t$, the variations are about 7% and 5% for case (1), 3% and less than 1% for case (2), 9% and 5% for case (3), at the LO and NLO, respectively.

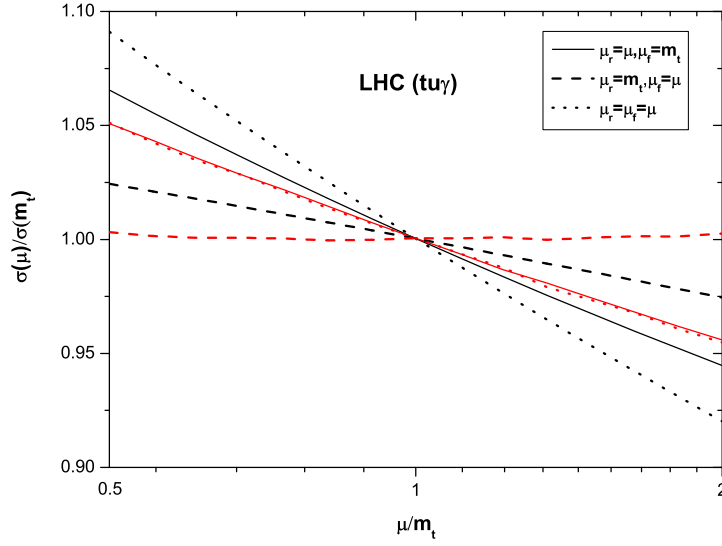


FIG. 6: Scale dependence of the total cross sections at the LHC, the black lines represent the LO results, while the red lines represent the NLO results.

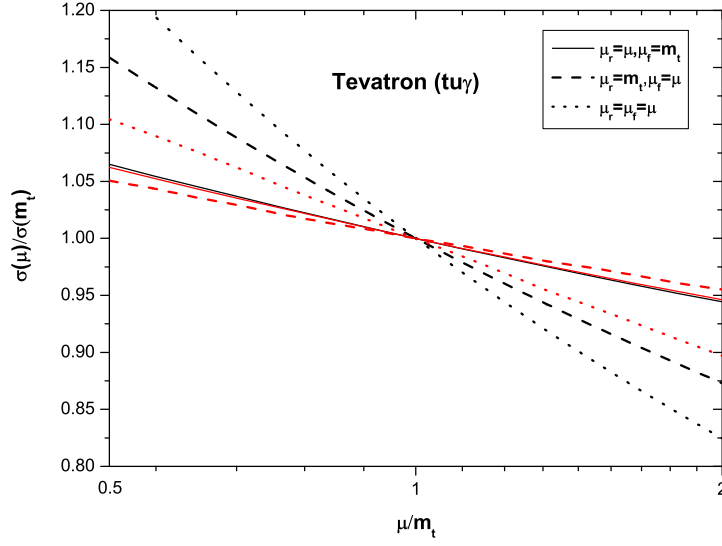


FIG. 7: Scale dependence of the total cross sections at the Tevatron, the black lines represent the LO results, while the red lines represent the NLO results.

Fig. 8 and 9 give the transverse momentum distributions of the photon and the final state top quark, respectively. We can see that the NLO corrections increase the distributions of the FCNC top quark associated γ production in both high and low p_T regions. Fig. 10 shows the invariant mass distributions of the photon and the top quark, where there is a peak in the middle region in the invariant mass distributions of this process. The NLO corrections do not change the shapes of these distributions.

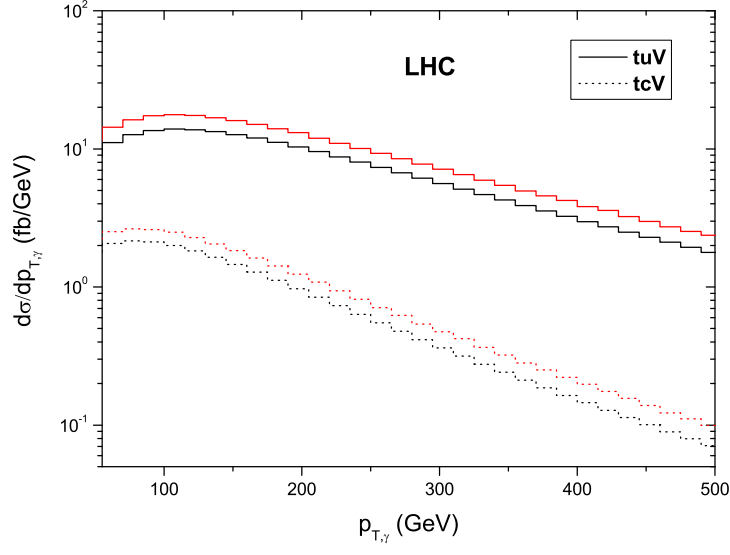


FIG. 8: Transverse momentum distributions of the photon, the black and red line represent the LO and NLO results of the FCNC top quark associated γ production, respectively.

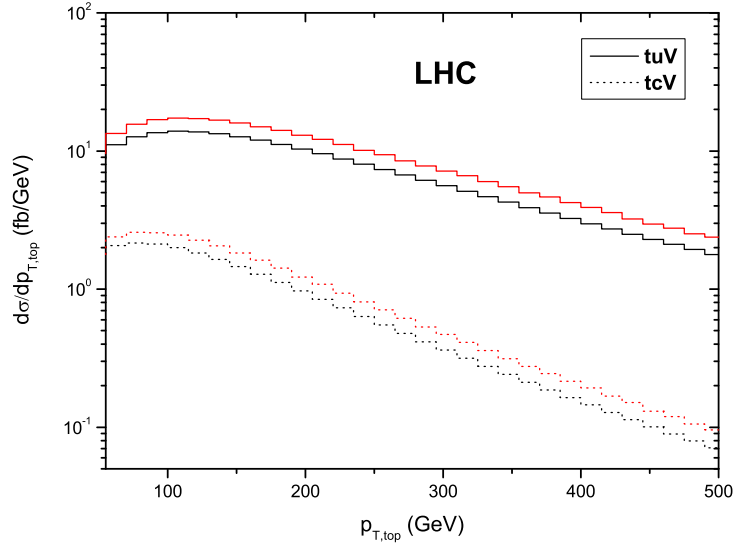


FIG. 9: Transverse momentum distributions of the top quark, the black and red line represent the LO and NLO results of the FCNC top quark associated γ production, respectively.

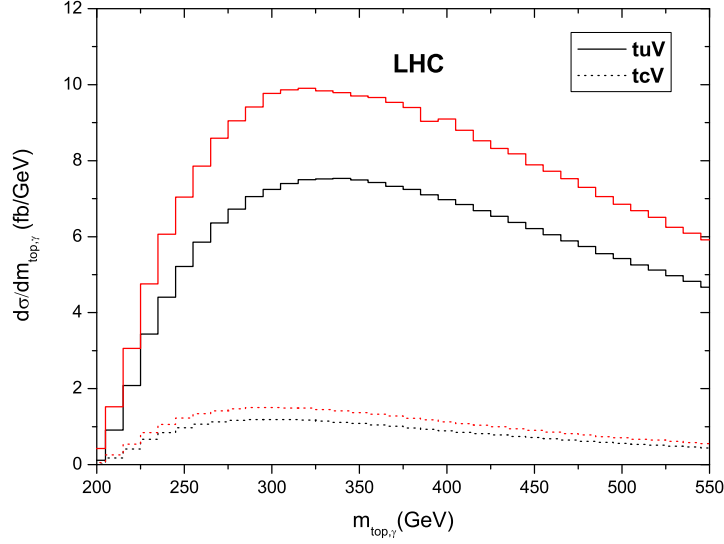


FIG. 10: Invariant mass distributions of the photon and the top quark, the black and red line represent the LO and NLO results of the FCNC top quark associated γ production, respectively.

B. Combination of the contributions from the $tq\gamma$ and tqg FCNC couplings with mixing effects

In this subsection, we present the numerical results of the single top associated with γ production via the electroweak and strong FCNC couplings, including the NLO QCD effects and the mixing effects. For the numerical calculations, we take the same SM parameters and kinematical cuts as above subsection, and set the values of the FCNC couplings as follows:

$$\kappa_{tu}^{\gamma}/\Lambda = \kappa_{tc}^{\gamma}/\Lambda = 0.02\text{TeV}^{-1}, \quad \kappa_{tu}^g/\Lambda = \kappa_{tc}^g/\Lambda = 0.01\text{TeV}^{-1}. \quad (32)$$

In Table II, we show some typical numerical results of the LO and NLO total cross sections for process induced by both the electroweak and strong FCNC couplings with the mixing effects.

From above results, we can see that the NLO effects are more significant in the process induced by tcV FCNC couplings than in one induced by tuV FCNC coupling. This is because that the contributions from $gg \rightarrow \gamma t\bar{c}$ subprocess is exactly the same as $gg \rightarrow \gamma t\bar{u}$ subprocess, while the difference of the corresponding LO cross sections between the above two processes

FCNC coupling	tuV (LO)	tuV (NLO)	tcV (LO)	tcV (NLO)
LHC $(\frac{\kappa/\Lambda}{0.01\text{TeV}^{-1}})^2$ fb	27.8	42.7	3.13	5.61

TABLE II: The LO and NLO total cross sections for process induced by the $tq\gamma$ and tqg FCNC couplings with mixing effects at the LHC. Here $f_{tq}^{\gamma*} f_{tq}^g + h_{tq}^{\gamma*} h_{tq}^g = 1$.

is nearly 10 times. For example, at the LHC, contributions from $gg \rightarrow \gamma t\bar{u}$ subprocess are about 3% of the corresponding LO cross section of $ug \rightarrow \gamma t$, while the contributions from $gg \rightarrow \gamma t\bar{c}$ subprocess are about 30% of the corresponding LO cross section of $cg \rightarrow \gamma t$.

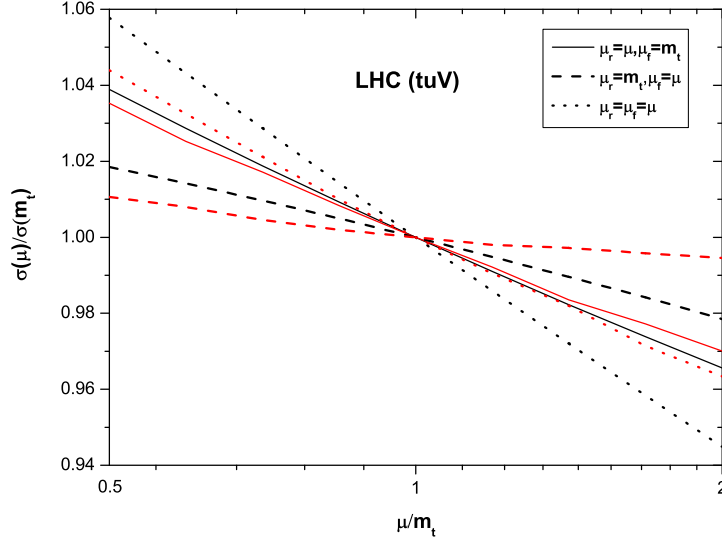


FIG. 11: Scale dependence of the total cross sections at the LHC, the black lines represent the LO results, while the red lines represent the NLO results. Here $\kappa_{tu}^{\gamma} = 2\kappa_{tu}^g$.

Fig. 11 shows the scale dependence of the total cross sections for the top quark associated with γ production via the FCNC couplings with the mixing effects at the LHC. We can see that the NLO QCD corrections reduce the dependence of the total cross sections on the renormalization and factorization scale significantly, as same as the case without the mixing effects.

After considering the mixing effects, the total cross sections of the top quark associated

with γ production via FCNC couplings can be factorized as:

$$\sigma = A\left(\frac{\kappa_{tq}^\gamma}{\Lambda}\right)^2 + B\left(\frac{\kappa_{tq}^g}{\Lambda}\right)^2 + C\left(\frac{\kappa_{tq}^\gamma}{\Lambda}\right)\left(\frac{\kappa_{tq}^g}{\Lambda}\right)\text{Re}(f^{\gamma*}f^g + h^{\gamma*}h^g). \quad (33)$$

where A, B and C represent the contributions from different couplings and mixing effects.

And, their numerical expressions at the LHC can be written as

$$\sigma_{LO}^{tuV} = \left[42.0\left(\frac{\kappa_{tu}^\gamma}{\Lambda}\right)^2 + 57.6\left(\frac{\kappa_{tu}^g}{\Lambda}\right)^2 + 26.4\left(\frac{\kappa_{tu}^\gamma}{\Lambda}\right)\left(\frac{\kappa_{tu}^g}{\Lambda}\right)\text{Re}(f^{\gamma*}f^g + h^{\gamma*}h^g) \right] \text{pb} \cdot \text{TeV}^2, \quad (34)$$

$$\sigma_{NLO}^{tuV} = \left[57\left(\frac{\kappa_{tu}^\gamma}{\Lambda}\right)^2 + 129\left(\frac{\kappa_{tu}^g}{\Lambda}\right)^2 + 35\left(\frac{\kappa_{tu}^\gamma}{\Lambda}\right)\left(\frac{\kappa_{tu}^g}{\Lambda}\right)\text{Re}(f^{\gamma*}f^g + h^{\gamma*}h^g) \right] \text{pb} \cdot \text{TeV}^2; \quad (35)$$

$$\sigma_{LO}^{tcV} = \left[4.3\left(\frac{\kappa_{tc}^\gamma}{\Lambda}\right)^2 + 9.5\left(\frac{\kappa_{tc}^g}{\Lambda}\right)^2 + 2.3\left(\frac{\kappa_{tc}^\gamma}{\Lambda}\right)\left(\frac{\kappa_{tc}^g}{\Lambda}\right)\text{Re}(f^{\gamma*}f^g + h^{\gamma*}h^g) \right] \text{pb} \cdot \text{TeV}^2, \quad (36)$$

$$\sigma_{NLO}^{tcV} = \left[6.0\left(\frac{\kappa_{tc}^\gamma}{\Lambda}\right)^2 + 24.1\left(\frac{\kappa_{tc}^g}{\Lambda}\right)^2 + 4.0\left(\frac{\kappa_{tc}^\gamma}{\Lambda}\right)\left(\frac{\kappa_{tc}^g}{\Lambda}\right)\text{Re}(f^{\gamma*}f^g + h^{\gamma*}h^g) \right] \text{pb} \cdot \text{TeV}^2. \quad (37)$$

In order to investigate the contributions from the mixing effects as shown in Eqs. (34), (35), (36) and (37), we present the contour curves for the variables $\text{Re}(f^{\gamma*}f^g)$ and $\text{Re}(h^{\gamma*}h^g)$, as shown in Fig. 12. It can be seen that the total cross sections at the NLO with the mixing effects increase slowly with increasing of $\text{Re}(f^{\gamma*}f^g)$ and $\text{Re}(h^{\gamma*}h^g)$.

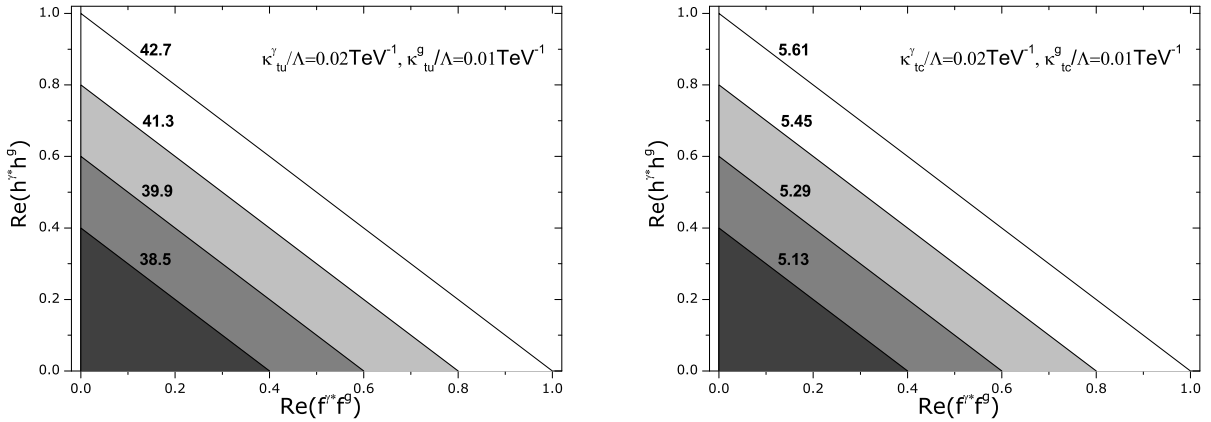


FIG. 12: The contour curves of the total cross sections (fb) of the top quark associated γ production at the NLO including the mixing effects versus the variables $\text{Re}(f^{\gamma*}f^g)$ and $\text{Re}(h^{\gamma*}h^g)$. The left diagram represents the process induced by tuV couplings. And the right one shows the process induced by tcV couplings.

VI. CONCLUSIONS

We have calculated the NLO QCD corrections to the top quark associated with γ production via the $tq\gamma$ and tqg FCNC couplings at hadron colliders, respectively, and we also consider the mixing effects. Our results show that, the NLO QCD corrections can enhance the total cross sections by about 50% and 40% for the $tq\gamma$ couplings at the Tevatron and LHC, respectively. If we combine the contributions from the $tq\gamma$, tqg FCNC couplings and the mixing effects, the NLO QCD corrections can enhance the total cross sections by about 50% for the $tu\gamma$ and tug FCNC couplings, and by about 80% for the $tc\gamma$ and tcg FCNC couplings at the LHC. Moreover, the NLO QCD corrections reduce the dependence of the total cross sections on the renormalization or factorization scale significantly, which leads to increased confidence in our theoretical predictions based on these results. Besides, we also evaluate the NLO QCD corrections to several important kinematic distributions, i.e., the transverse momentum of the photon and the top quark, and the invariant mass of the photon and the top quark, respectively. We find that the NLO corrections are almost the same and do not change the shape of the distributions.

Acknowledgments

This work was supported in part by the National Natural Science Foundation of China, under Grants No. 10975004, and No. 11021092.

-
- [1] S. L. Glashow, J. Iliopoulos and L. Maiani, Phys. Rev. D **2**, 1285 (1970).
 - [2] F. del Aguila, J. A. Aguilar-Saavedra and R. Miquel, Phys. Rev. Lett. **82**, 1628 (1999); J. A. Aguilar-Saavedra, Phys. Rev. D **67**, 035003 (2003) [Erratum-ibid. D **69**, 099901 (2004)].
 - [3] T. P. Cheng and M. Sher, Phys. Rev. D **35** 3484 (1987); M. E. Luke and M. J. Savage, Phys. Lett. B **307** 387 (1993); D. Atwood, L. Reina and A. Soni, Phys. Rev. D **55** 3156 (1997); S. Bejar, J. Guasch and J. Sola, Nucl. Phys. B **600** 21 (2001).
 - [4] C. S. Li, R. J. Oakes and J. M. Yang, Phys. Rev. D **49** 293 (1994) [Erratum-ibid. D **56** 3156 (1997)]; J. L. Lopez, D. V. Nanopoulos and R. Rangarajan, Phys. Rev. D **56** 3100 (1997); G. M. de Divitiis, R. Petronzio and L. Silvestrini, Nucl. Phys. B **504** 45 (1997); J. M. Yang,

- B. L. Young and X. Zhang, Phys. Rev. D **58** 055001 (1998); J. Guasch and J. Sola, Nucl. Phys. B **562** 3 (1999); G. Eilam, A. Gemintern, T. Han, J. M. Yang and X. Zhang, Phys. Lett. B **510** 227 (2001); J. j. Cao, Z. h. Xiong and J. M. Yang, Phys. Rev. Lett. **88** 111802 (2002); J. J. Liu, C. S. Li, L. L. Yang and L. G. Jin, Phys. Lett. B **599** 92 (2004).
- [5] H. Davoudiasl and T. G. Rizzo, Phys. Lett. B **512** 100 (2001); P. M. Aquino, G. Burdman and O. J. P. Eboli, Phys. Rev. Lett. **98** 131601 (2007); S. Casagrande, F. Goertz, U. Haisch, M. Neubert and T. Pfoh, JHEP **0810** 094 (2008); J. Gao, C. S. Li, X. Gao and Z. Li, Phys. Rev. D **78** 096005 (2008).
- [6] H. Hong-Sheng, Phys. Rev. D **75** 094010 (2007); X. Wang, Y. Zhang, H. Jin and Y. Xi, Nucl. Phys. B **810** 226 (2009); X. F. Han, L. Wang and J. M. Yang, arXiv:0903.5491 [hep-ph].
- [7] X. L. Wang, G. R. Lu, J. M. Yang, Z. J. Xiao, C. X. Yue and Y. M. Zhang, Phys. Rev. D **50** 5781 (1994); G. Burdman, Phys. Rev. Lett. **83** 2888 (1999); C. x. Yue, G. r. Lu, Q. j. Xu, G. l. Liu and G. p. Gao, Phys. Lett. B **508** 290 (2001); J. j. Cao, G. l. Liu and J. M. Yang, Phys. Rev. D **70** 114035 (2004); J. j. Cao, G. l. Liu, J. M. Yang and H. j. Zhang, Phys. Rev. D **76** 014004 (2007).
- [8] M. Beneke *et al.*, arXiv:hep-ph/0003033.
- [9] F. Abe *et al.* [CDF Collaboration], Phys. Rev. Lett. **80**, 2525 (1998).
- [10] J. J. Zhang, C. S. Li, J. Gao, H. Zhang, Z. Li, C. P. Yuan and T. C. Yuan, Phys. Rev. Lett. **102**, 072001 (2009).
- [11] J. J. Zhang, C. S. Li, J. Gao, H. X. Zhu, C. P. Yuan and T. C. Yuan, Phys. Rev. D **82**, 073005 (2010).
- [12] S. Chekanov *et al.* [ZEUS Collaboration], Phys. Lett. B **559**, 153 (2003).
- [13] A. Belyaev and N. Kidonakis, Phys. Rev. D **65**, 037501 (2002).
- [14] V. M. Abazov *et al.* [D0 Collaboration], Phys. Lett. B **693**, 81 (2010).
- [15] T. Aaltonen *et al.* [CDF Collaboration], Phys. Rev. Lett. **102**, 151801 (2009).
- [16] J. J. Liu, C. S. Li, L. L. Yang and L. G. Jin, Phys. Rev. D **72**, 074018 (2005).
- [17] J. Gao, C. S. Li, J. J. Zhang and H. X. Zhu, Phys. Rev. D **80**, 114017 (2009).
- [18] L. L. Yang, C. S. Li, Y. Gao and J. J. Liu, Phys. Rev. D **73**, 074017 (2006).
- [19] J. A. Aguilar-Saavedra, Acta Phys. Polon. B **35**, 2695 (2004); J. A. Aguilar-Saavedra, Nucl. Phys. B **837**, 122 (2010); N. Kidonakis and A. Belyaev, JHEP **0312**, 004 (2003).
- [20] S. Catani and M. H. Seymour, Nucl. Phys. B **485**, 291 (1997) [Erratum-ibid. B **510**, 503

(1998)].

- [21] S. Catani, S. Dittmaier, M. H. Seymour and Z. Trocsanyi, Nucl. Phys. B **627**, 189 (2002).
- [22] B. W. Harris and J. F. Owens, Phys. Rev. D **65**, 094032 (2002).
- [23] S. Frixione, Phys. Lett. B **429**, 369 (1998).
- [24] K. Nakamura *et al.* [Particle Data Group], J. Phys. G **37**, 075021 (2010).
- [25] J. Pumplin, D. R. Stump, J. Huston, H. L. Lai, P. M. Nadolsky and W. K. Tung, JHEP **0207**, 012 (2002).
- [26] R. Frederix, T. Gehrmann and N. Greiner, JHEP **0809**, 122 (2008).

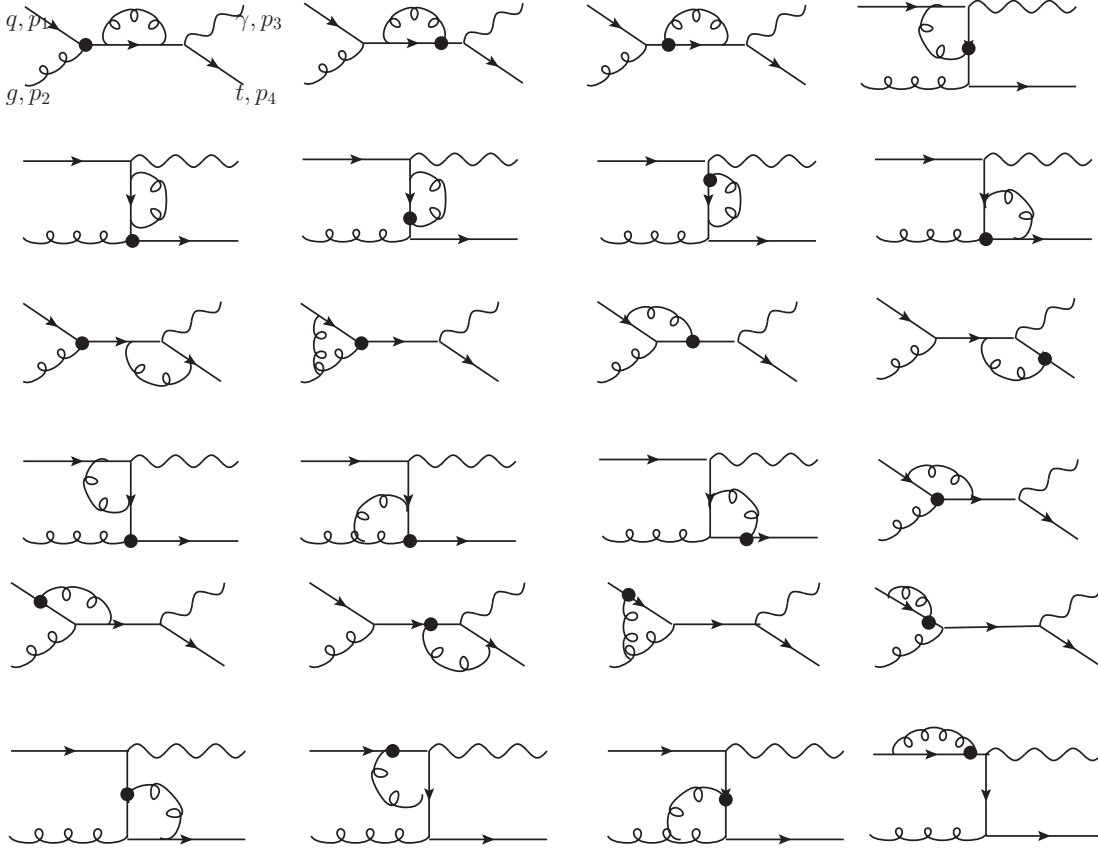


FIG. 13: One-loop Feynman diagrams induced by the tqg FCNC couplings, part I.

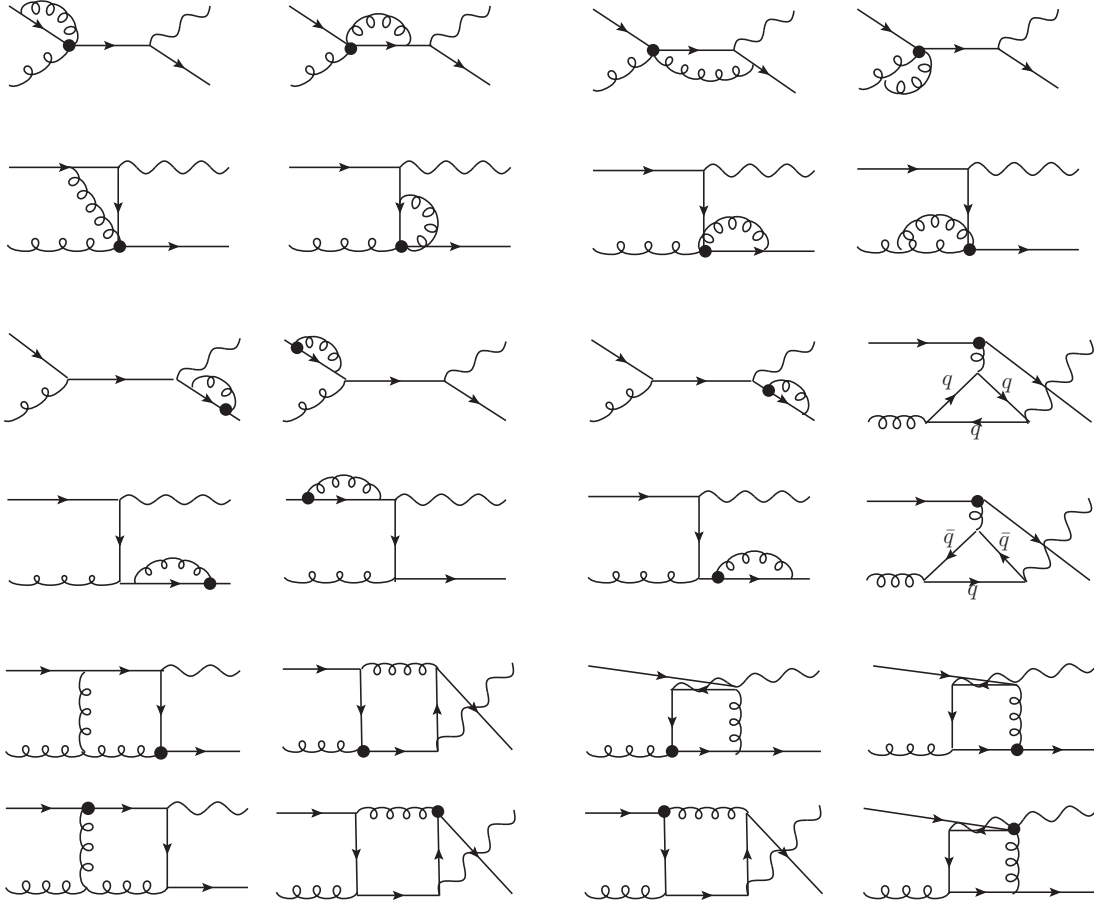


FIG. 14: One-loop Feynman diagrams induced by the tqg FCNC couplings, part II.

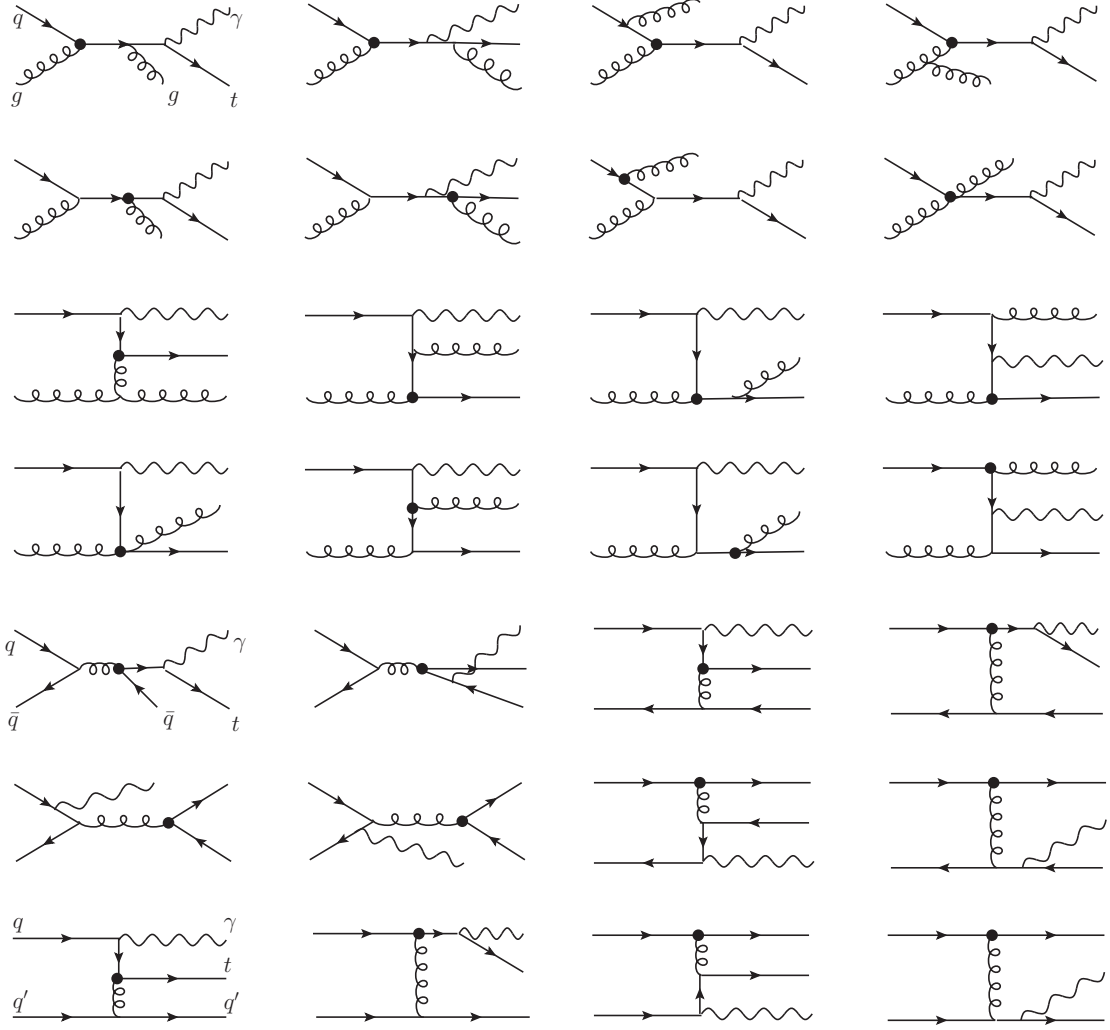


FIG. 15: Feynman diagrams of the real corrections induced by the tqg FCNC couplings, part I.

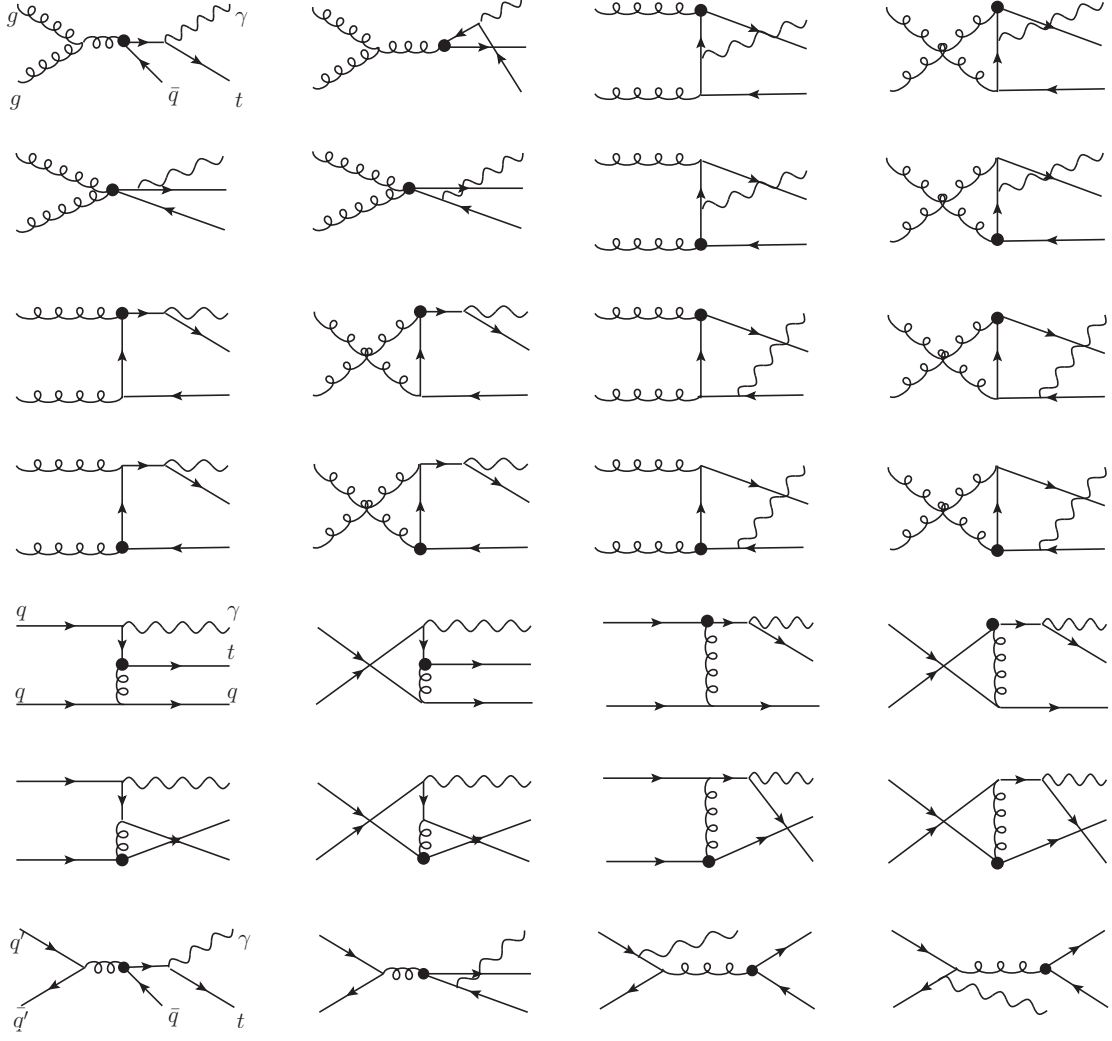


FIG. 16: Feynman diagrams of the real corrections induced by the tqg FCNC couplings, part II.